Article

Large-Scale, Cuttable, Full Tissue-Based Capacitive Pressure Sensor for the Detection of Human Physiological Signals and Pressure Distribution

Xin He,* Xiang He, Houlong He, Shunli Liang, Zhihao Liu, Jionghong Liang, Yue Xin, Weijia Yang, Yan Chen, and Chi Zhang

ACCESS | Metrics & More | Article Recommendations | SI Supporting Information

ABSTRACT: The increasing demand for flexible and wearable electronics has promoted the rapid development of the pressure sensors capable of monitoring diverse human movements and physiological signals. However, more and more research requires the pressure sensor to possess high sensing performance and desires the fabrication to exhibit the characteristics of low cost, large-scale production, high reproduction, even disposability. Here, we propose a full tissue-based capacitive pressure sensor with a sandwiched structure consisting of two MXene-coated tissue electrodes and a blank tissue dielectric layer. The tight contact and adequate adsorption of the MXene sheets with the cellulose fibers endow the electrode with uniform conductivity and high stability over a large area. In addition, the flexible sensor could be conveniently cut into any shape and size to meet the diverse application requirements. Thereby, the pressure sensor exhibits a sensitivity of 0.051 kPa^{-1} (<7 kPa), a wide detection range of 0.02−160 kPa, a fast response (∼100 ms), and good repeatability. The flexible device has been demonstrated to monitor a variety of human activities and physical stimuli. The assembled sensor array can accurately and reliably detect the pressure distribution.
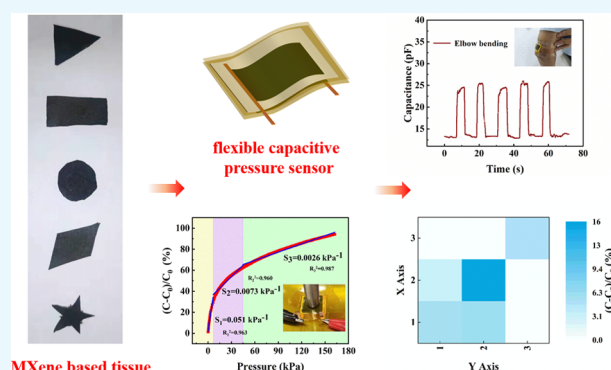
1. INTRODUCTION

With the rapid development of the Internet of Things and artificial intelligence, flexible electronics have attracted more and more attention.[1] Accordingly, the market share of smart and wearable devices has been increasing quickly.[2−6] As one of the significantly wearable devices, the stress sensor comprises the advantages of high flexibility, portability, and integrability with other flexible electronic devices.[7−9] According to the signal conversion mechanisms, the flexible stress sensor can be divided into four types, including resistive,[10,11] capacitive,[12,13] piezoelectric,[14,15] and triboelectric type.[16] The capacitive stress sensor has received intense investigations due to its simple structure, facile fabrication, high adaptability, fast response, and excellent stability.[17]

The capacitive sensors generally are fabricated with a sandwiched structure, consisting of upper/lower electrodes and a dielectric layer.[18] The electrode composed of conducting active materials and flexible supporting layer plays a vital role in determining the sensor performance. On the one hand, the conductive materials, including metal nanoparticles/nanowires,[19−23] carbon-based materials,[24−26] MXene (Ti$_3$C$_2$T$_x$),[27−32] indium tin oxide (ITO),[33,34] and conducting polymers,[35,36] have been widely used in the flexible capacitive stress sensors. On the other hand, the supporting layer

materials of the electrode, such as poly(dimethylsiloxane) (PDMS),[37,38] polyimide (PI),[39] Ecoflex,[40] poly(methyl methacrylate) (PMMA),[41] fibers,[42,43] and tissues,[44] are required to be highly flexible, superbly stable, and biocompatible. The fabrication of macromolecular polymers generally needs complicated curing processes and relatively high material costs. Additionally, the conducting networks are usually embedded in the organic layer to obtain good interfacial contact between the conducting materials and the organic layer via a curing-transfer method.[45] However, this technology often results in the uneven distribution of the conducting materials on the electrode surface due to the incomplete transfer.

Therefore, it is highly desirable to explore a flexible electrode of the stress sensors with the merits of low cost, simple fabrication process, high uniformity, and scale-up technology. To achieve it, the flexible and low-cost fibers or tissues are
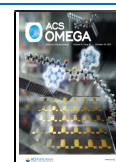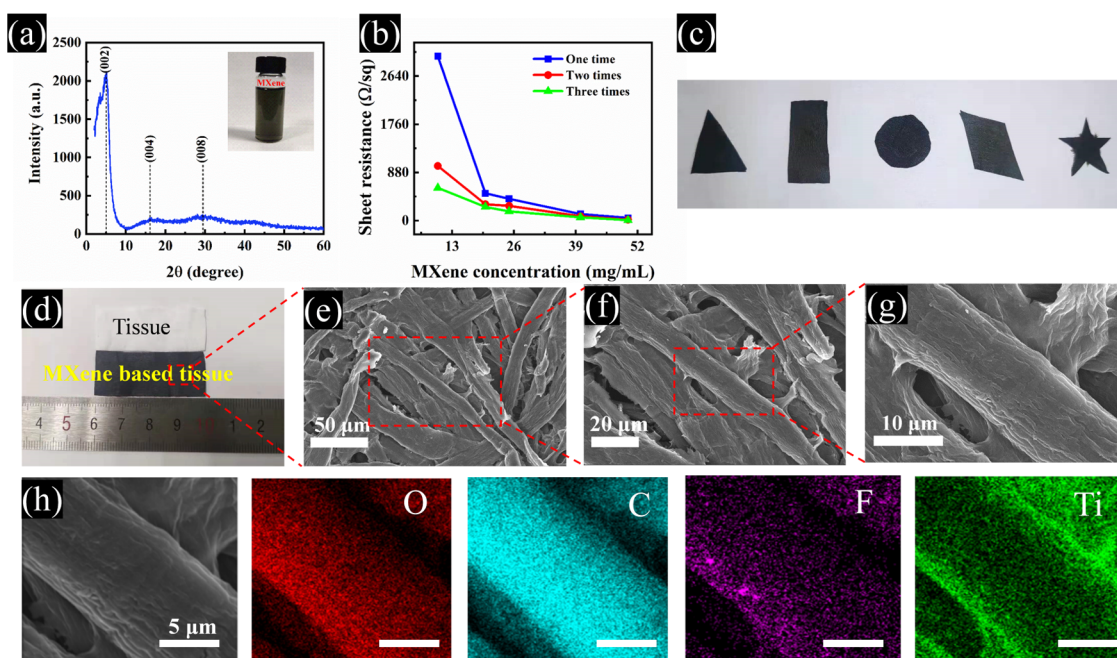
Figure 1. (a) XRD pattern of the multilayered MXene. (b) Relationship between MXene concentration and sheet resistance of the electrode with different soaking times. (c) Photographs of the tissue-supporting electrode with various sizes and shapes. (d) Photographs of the tissue paper before and after adsorbing the MXene sheets. (e−g) Scanning electron microscopy (SEM) images of the electrode with different magnifications. (h) Corresponding element mapping images of the electrode.

ideal candidates for the supporting layers of the sensor electrode. For example, Zhang et al. proposed a pressure sensor based on MXene-textile prepared by a dip-coating process.[46] The device exhibited the highest sensitivity of 12.095 kPa^{-1} in the range of 29−40 kPa, a rapid response time of 26 ms, and a detected range of 40 kPa. Kannichankandy et al. reported a device using polyaniline (PANI) incorporated with cellulose paper (CP) substrate by dip-coating, delivering a sensitivity of 2.23 kPa^{-1} and a fast response of 70 ms, and an operating range of 2−90 kPa.[47]

Although the fabrication of pressure sensors based on cotton fabrics and tissue papers could reduce the cost and complexity of the technology, the device performances (such as detect pressure range) and large-scale fabrication still demand further improvement to meet the wide application requirements.[43] Herein, we proposed a full tissue-based capacitive pressure sensor using MXene sheets-coated tissue as the electrodes and blank tissue as the dielectric layer. There are four advantages of the fabricated device. First, the tissue paper as the supporting layer can adequately adsorb the MXene sheets owing to its intense hygroscopic property and rough fiber surfaces, realizing uniform conductivity of the electrode over a large area. Second, the two-dimensional structure of MXene sheets can tightly contact the cellulose fibers, achieving the high mechanical stability of the device under repeated loading. Third, the air gaps among the tissue fibers enable a relatively significant capacitance change under external loading, improving the sensing ability. Fourth, the device can be cut into any desired shape and size, exhibiting a facile and low-cost fabrication. As a result, the full tissue-based capacitive pressure sensor delivered the highest sensitivity of 0.051 kPa^{-1} (<7 kPa), the wide detection range of 0.02−160 kPa, and rapid response (∼100 ms). In addition, the sensor demonstrated the detection of a variety of human movements in real-time, and the sensor array could be used to describe the pressure distribution.

2. RESULTS AND DISCUSSION

X-ray diffraction (XRD) detected the structure of the MAX phase after etching with 2θ ranged from 2.5 to 60° (Figure 1a). The dominant diffraction peak of the pattern at 5.1° indexed to the (002) plane of layer-structured MXene. Additionally, the characteristic peak of Al around 40° disappeared, denoting that the Al layer of the MAX phase has been completely etched. Figure S1 provides the morphological change of the MAX phase before and after etching, verifying the formation of the multilayered MXene. Furthermore, the multilayered MXene was delaminated with the assistance of ultrasonic treatment to obtain a few-layered MXene, whose sheet-like structure is beneficial to be adequately and tightly adsorbed by the tissue paper fibers. Figure 1b displays the variation trend of electrode sheet resistance as the MXene concentration and soaking time. The electrode resistivity gradually decreased as MXene concentration and soaking time increased, indicating that the electrode conductivity was controllable. When the adsorption of conducting materials reaches saturation, the electrode sheet resistance kept the lowest value of 17 Ω/sq. We applied a constant loading of 2 N to the tissue-based electrode directly. The changes of electrode resistance were maintained below ∼30% during 2000 loading−unloading cycles. The printing paper placed under the electrode showed no noticeable residue of MXene after repeated loading, revealing excellent adhesion of MXene sheets to tissue internetworks (Figure S2).

The obtained electrode exhibited a deep black color (Figure S3 shows the electrode color with different soaking times) and could be facilely cut into different sizes and shapes to meet diverse application requirements (Figure 1c). Figure 1d manifests that the tissue paper retains a similar size before and after adequately adsorbing the MXene sheets. Figure 1e−g shows the micromorphology of the tissue-supporting electrode with various magnifications, indicating that the electrode is composed of one-dimensional fibers. The MXene sheets cover
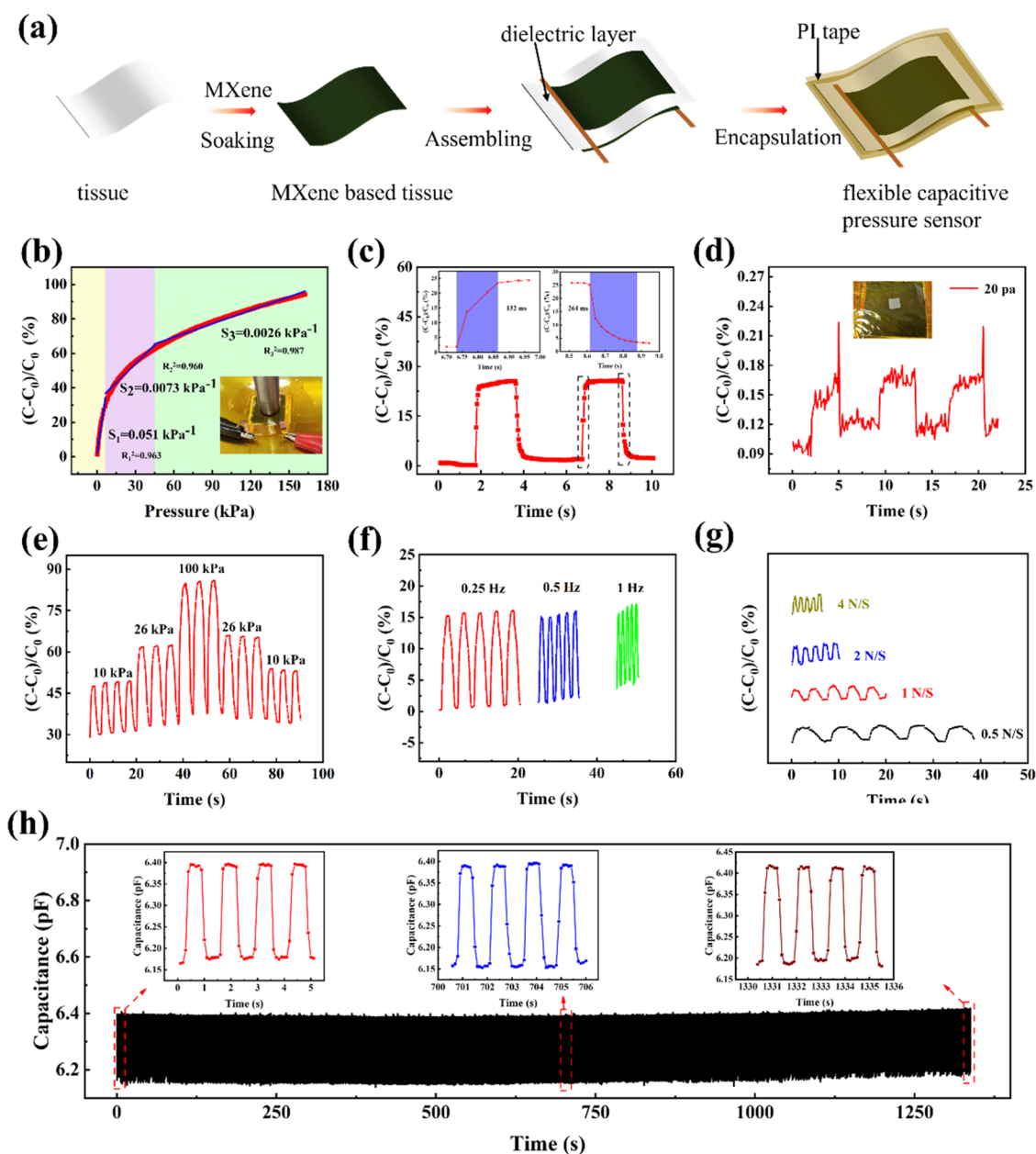
Figure 2. (a) Schematic presentation of the fabrication process of a full tissue-based capacitive pressure sensor. (b) Capacitance changes of the sensor under the external pressure of 0−160 kPa, and the inset shows the measurement picture. (c) Dynamic response and relaxation time of the sensor, and the insets are local enlarged curves. (d) Test of the sensor's capability to detect a lightweight iron sheet with a pressure of 20 Pa, and the inset is the corresponding picture; capacitance responses of the sensor with different external forces of 10, 26, and 100 kPa (e), loading frequencies of 0.25, 0.5, and 1 Hz (f), and loading rates of 0.5, 1, 2, and 4 N/s (g). (h) Long-term stability test of the sensor under a constant force of 4 N for 1000 cycles.

the fiber surfaces and occupy the space among the fibers due to the strong absorptivity of the cellulose fibers. The corresponding element mapping images confirm that O, C, F, and Ti elements from MXene sheets are distributed on the fibers (Figure 1h). In addition, a large-area electrode was prepared by soaking the tissue with the area of 50 mm × 150 mm into the MXene solution to investigate the resistance uniformity. The 14 cut electrodes with 20 mm × 25 mm dimensions exhibited an average resistance of 68.6 Ω, and a standard deviation of 11%, revealing a relatively uniform distribution in the conductivity (Figure S4).

Figure 2a presents the fabrication process of the full tissue-based capacitive pressure sensor. Typically, two pieces of

MXene-coated tissues with an area of 20 mm × 25 mm were used as the upper and lower electrodes, while a piece of blank tissue with a size of 23 mm × 26 mm served as the dielectric layer. Two electrodes and the intermediate dielectric layer were assembled into a sandwiched device, delivering the characteristics of thinness, high flexibility, low-cost fabrication, and cuttability. The PI tape was utilized to encapsulate the whole device, ensuring capacitance stability under different humidities (Figure S5).

To ascertain the sensing ability of the full tissue-based sensor in response to the external pressures, we used a measurement system consisting of a universal electronic testing machine and LCR instrument to detect the device capacitance under
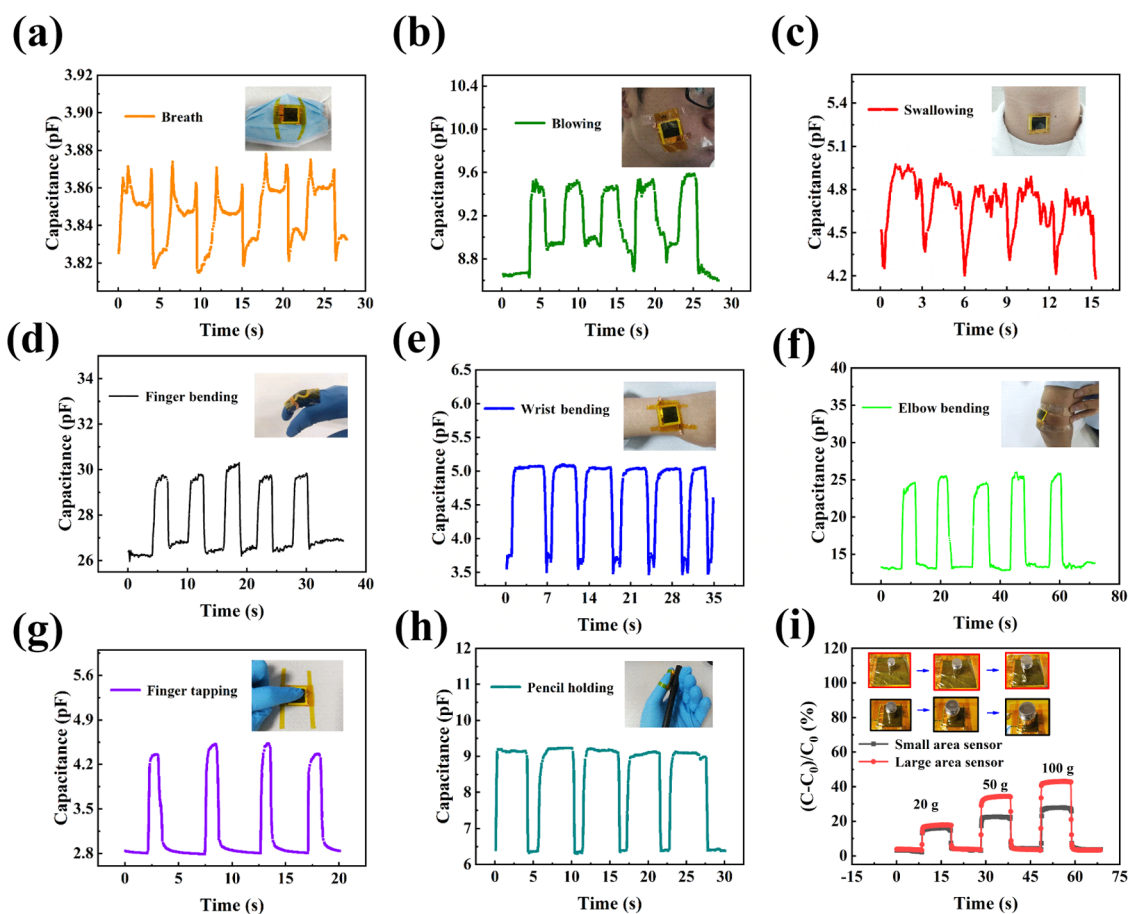
Figure 3. Demonstration of the full tissue-based sensor as a tactile device. Detecting human physiological signals from the breath (a), air blowing (b), and swallowing (c). Monitoring the joint bending, including the bending of the finger (d), wrist (e), and elbow (f). Detecting the real-time capacitance changes in response to the finger-tapping (g), pencil holding (h), and weight pressing (i).

different loading pressures. Figure 2b shows the relative capacitance changes of the sensor within the wide pressure range. The sensitivity of the capacitive sensor is determined by the equation of $S = (\Delta C/C_0)/\Delta P$, where ΔC represents the variation of capacitance value ($\Delta C = C - C_0$), C is the capacitance at a loading state, C_0 is the initial capacitance without loading, and ΔP is the pressure change.[48,49] The sensitivity of the full tissue-based sensor exhibits three distinct linear regions in the pressure range of 0−7, 7−45, and 45−160 kPa, corresponding to the sensitivity of 0.051, 0.0073, and 0.0026 kPa^{-1}, respectively. Usually, the capacitance change should be as significant as possible under a loading state to realize a high sensitivity for the capacitive sensor. According to the capacitance definition of the plate capacitor $C = \varepsilon S/4\pi k d$, where ε corresponds to the dielectric constant, d is the distance between the two plates, k refers to the electrostatic constant, and S represents the area of the capacitor plate, the device capacitance could be altered by changing the structure parameters.[50] In this work, the tissue paper exhibits porous microstructure due to the interconnection of the cellulose fibers. When the external force was applied to the sensor, the internal air pores among the fibers were compressed, resulting in a remarkable decrease of d and an increase of ε, especially in the case of low-pressure loading.[51] The air pore compression gradually attained saturation as the pressure increased. Meanwhile, the contact area between the MXene sheets on the fiber surface also increased as the exerted force elevated, improving the effective area S of conducting materials.

Therefore, the changes of d, ε, and S increased sensor capacitance variation together.

The response time of the capacitive pressure sensor was evaluated by a typical time−capacitance cycle curve (Figure 2c). The local enlarged curves in the insets indicate that the rise and fall times of the sensor were 132 and 264 ms, respectively. The ability to detect a low stimulus is one of the crucial indicators for stress sensors. Figure 2d displays the repeated signal stemming from loading/unloading an iron sheet. A slight pressure of 20 Pa was clearly identified, revealing that our sensor could reliably detect low stimulus by the capacitive response. Mechanical stability is another significant factor for determining the performance of flexible sensors. We measured the capacitance changes in response to the stepped increase and decrease of pressures (10, 26, and 100 kPa) (Figure 2e). The stable signal output denotes that the sensor can work under different pressures and maintain excellent symmetric responses under the same loadings.

Figure 2f,g shows the cyclic capacitance changes of the sensor with different loading frequencies of 0.25, 0.5, and 1 Hz and loading rates of 0.5, 1, 2, and 4 N/s. The sensor exhibits fast response and high recoverability regardless of the loading frequency and rate. It also reflects that the sensor possesses excellent resolution ability of the frequency and stably operates within a wide range of loading rates. The long-term stability of the sensor was evaluated by dynamically loading/unloading a constant force of 4 N for 1000 cycles (Figure 2h). The capacitance could recover the initial value after repeated
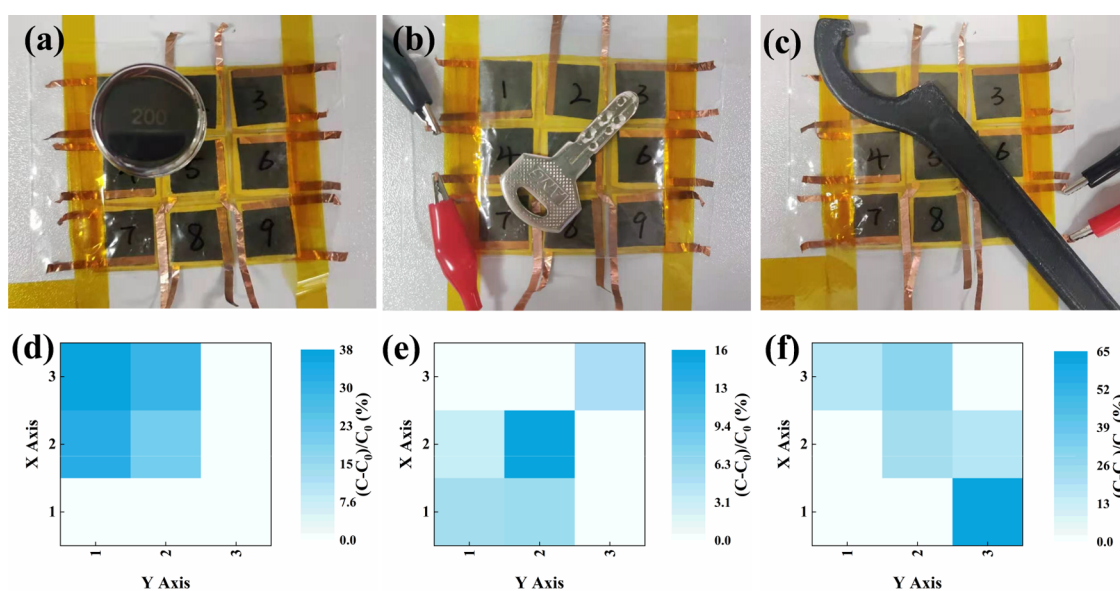
Figure 4. Photographs of the 3 × 3 pixels pressure sensor array with loading a standard weight of 200 g (a), key (b), and spanner (c), respectively. (d−f) The corresponding mapping of the capacitance change and pressure distribution.

loading, and the signal amplitude remained the same, demonstrating the good robustness of whole tissue-based device. The insets of Figure 2h are the cyclic curves at the initial, intermediate, and final stages, confirming highly stable capacitance changes during the long-term cyclic test.

Based on the above performance measurement analysis, our sensor exhibits the advantages of high sensitivity, especially in low-pressure range, fast response, wide operating range, and good stability. To further assess the application of a full tissue-based pressure sensor as a practical and versatile wearable device, we attached the sensor to the human body parts to monitor various movements in real-time. The sensor was adhered to a mask to detect human respiration (Figure 3a). The exhaled air generated a slight pressure on the sensor, increasing sensor capacitance, and then the capacitance returned to its original value on inhalation. Thus, the sensor could detect a stable capacitance signal that responded to the breath, which was expected to monitor sleep apnea to avoid suffocation for the patients. The sensor was also able to detect the movements of human muscles such as cheek (Figure 3b) and Adam's apple (Figure 3c) in real-time. The repeated capacitance waveforms suggest that the attached sensor has responded to the actions of air blowing and swallowing. Additionally, the flexible device was fixed to the joints of the human body, such as the finger (Figure 3d), wrist (Figure 3e), and elbow (Figure 3f), to detect joint bending. The joints were bent to provide a certain pressure on the sensor; thus, the capacitance value accordingly increased. The bending angles could be evaluated by collecting the capacitance variations. The signals present rapid and stable responses to the bending of various joints, reflecting that the sensor can monitor the movement of small joints (such as a finger) and large joints (such as wrist and elbow).

We also tested the sensor response to other physical stimuli. The device immediately responded when a finger tapped the sensor, figuring the characteristic of rapid response and high sensitivity (Figure 3g). To explore the application in human−machine interaction, we fixed the sensor on the thumb. When we used a similar force to grab a pencil, the sensor capacitance

maintained a highly stable maximum for each cycle, demonstrating excellent recoverability (Figure 3h). In addition, we presented the sensing ability comparison of the sensors with the areas of 30 mm × 30 mm and 60 mm × 60 mm (Figure 3i), indicating that the two sensors offer a similar capacitance response to a relatively small loading (such as 20 g weight). Still, the large-area sensor has a more significant sensing ability under a heavier loading (such as 50 and 100 g weights) due to its larger initial capacitance and capacitance change. Therefore, the large-area sensor has a better sensing resolution in response to large external loading.

The full tissue-based capacitive sensor fabricated by a soaking−drying method exhibits the merits of uniform performance, low cost, and scale-up fabrication. Therefore, we used nine parallel sensors to prepare 3 × 3 pixels pressure sensor arrays, detecting spatial pressure distribution. A 200 g weight, key, and spanner were respectively placed on the sensor arrays to investigate the distinguishable ability of the sensor arrays to the object shape and pressure distribution. The photographs of the practical location of the objects are shown in Figure 4a−c. The corresponding sensor capacitances were collected and plotted as two-dimensional distribution mapping (Figure 4d,e). The increase in the sensor capacitance was observed at the sites of loading objects along with a deeper blue color, denoting a relatively higher pressure. The color contrast identified the object shapes from the pressure mappings, revealing an excellent spatial resolution of the sensor array.

3. EXPERIMENTAL SECTION

3.1. Materials. The commercial tissue paper was purchased from Vida Trading Co., Ltd. It is composed of cellulose, featuring the merits of softness, excellent toughness, and hygroscopic property. Hydrochloric acid (HCl) and lithium fluoride (LiF) were obtained from Guangzhou Chemical Reagent Factory and Alfa Aesar (China) Chemical Co., Ltd., respectively, while Ti_3AlC_2 (99.7%, 400 mesh) powder was provided by 11 Technology Co., Ltd.

3.2. Preparation of Few-Layered MXene Sheets.

MXene sheets were obtained using selective etching of the Al atomic layer of the MAX phase precursor powder and following the delamination process.[52] First, 1.6 g of LiF was gently added into 20 mL of 9 M HCl to produce hydrofluoric acid. Second, 1 g of Ti_3AlC_2 was introduced into the above solution under magnetic stirring to avoid a sudden increase in the reaction temperature. Then, the etching of the Al layer was conducted at 35 °C for 48 h under continuous stirring. Third, the obtained product was repeatedly washed using deionized water until the pH value of the supernatant reached 6. Finally, the precipitate was redispersed in water and underwent delamination with ultrasonic treatment for 2 h to further prepare few-layered MXene sheets.

3.3. Fabrication of Electrode and Device.

The MXene-based electrodes were obtained by a simple soaking and drying method. The commercial tissue paper as a supporting layer of the desired size was wholly immersed into the few-layered MXene dispersion for a while and then taken out to dry at 60 °C. The process of soaking and drying was repeated to control the electrode conductivity. The electrode could be cut into any shape according to the application requirements. The full tissue-based capacitive pressure sensor was assembled with a sandwich structure consisting of two MXene-based electrodes and a clean tissue dielectric layer. The device was finally encapsulated by polyimide (PI) tapes.

3.4. Characterization.

A scanning electron microscope (SEM) (Zeiss Sigma 500, Germany) was used to observe the surface morphology of the electrode and conduct the corresponding element mapping analysis. The structure of the etched product was characterized by X-ray diffraction (XRD) (X'pert Pro MFD, PANalytical, the Netherlands) with Cu Kα radiation (λ = 0.154178 nm). A universal electronic testing machine (LE, LiShi, China) provided various pressures to the sensor, and the capacitance responses of the full tissue-based sensor to the pressures were collected in real-time by inductance, capacitance, and resistance (LCR) measurement instrument (IM3536, HIOKI, Japan). The LCR testing frequency was set as 800 kHz.

4. CONCLUSIONS

This work developed a full tissue-based capacitive pressure sensor based on MXene-coated electrodes and the blank tissue dielectric layer. The fabricated device exhibited the merits of low cost, facile fabrication process, large-scale and uniform electrode, and excellent sensing performances. The applications of the proposed pressure sensor to detect various human movements have been evidenced, and the pressure distribution could be identified by a sensor array, exhibiting promising prospects in wearable devices.

■ ASSOCIATED CONTENT

ⓢ Supporting Information

The Supporting Information is available free of charge at https://pubs.acs.org/doi/10.1021/acsomega.1c03900.

> Morphology of MXene; photographs of the electrodes; and the mechanical stability/conductivity uniformity/humidity resistance of the MXene-based electrode (PDF)

■ AUTHOR INFORMATION

Corresponding Author

Xin He − School of Applied Physics and Materials, Wuyi University, Jiangmen 529020, P. R. China; ⓞ orcid.org/0000-0002-1018-3512; Email: hexinwyu@126.com

Authors

Xiang He − School of Applied Physics and Materials, Wuyi University, Jiangmen 529020, P. R. China

Houlong He − School of Applied Physics and Materials, Wuyi University, Jiangmen 529020, P. R. China

Shunli Liang − School of Applied Physics and Materials, Wuyi University, Jiangmen 529020, P. R. China

Zhihao Liu − School of Applied Physics and Materials, Wuyi University, Jiangmen 529020, P. R. China

Jionghong Liang − School of Applied Physics and Materials, Wuyi University, Jiangmen 529020, P. R. China

Yue Xin − School of Applied Physics and Materials, Wuyi University, Jiangmen 529020, P. R. China

Weijia Yang − School of Applied Physics and Materials, Wuyi University, Jiangmen 529020, P. R. China

Yan Chen − School of Applied Physics and Materials, Wuyi University, Jiangmen 529020, P. R. China

Chi Zhang − School of Applied Physics and Materials, Wuyi University, Jiangmen 529020, P. R. China; ⓞ orcid.org/0000-0002-4976-0276

Complete contact information is available at:
https://pubs.acs.org/10.1021/acsomega.1c03900

Notes

The authors declare no competing financial interest.

■ ACKNOWLEDGMENTS

■ REFERENCES

(1) Jung, B. K.; Jeon, S.; Woo, H. K.; Park, T.; Ahn, J.; Bang, J.; Lee, S. Y.; Lee, Y. M.; Oh, S. J. Janus-like jagged structure with nanocrystals for self-sorting wearable tactile sensor. ACS Appl. Mater. Interfaces 2021, 13, 6394−6403.

(2) Fan, X.; Nie, W.; Tsai, H.; Wang, N.; Huang, H.; Cheng, Y.; Wen, R.; Ma, L.; Yan, F.; Xia, Y. PEDOT:PSS for flexible and stretchable electronics: modifications, strategies, and applications. Adv. Sci. 2019, 6, No. 1900813.

(3) Gao, W.; Ota, H.; Kiriya, D.; Takei, K.; Javey, A. Flexible electronics toward wearable sensing. Acc. Chem. Res. 2019, 52, 523−533.

(4) Shi, Q.; Dong, B.; He, T.; Sun, Z.; Zhu, J.; Zhang, Z.; Lee, C. Progress in wearable electronics/photonics—Moving toward the era of artificial intelligence and internet of things. InfoMat 2020, 2, 1131−1162.

(5) Vu, C. C.; Kim, S. J.; Kim, J. Flexible wearable sensors - an update in view of touch-sensing. *Sci. Technol. Adv. Mater.* **2021**, *22*, 26−36.

(6) Wang, C.; Xia, K.; Wang, H.; Liang, X.; Yin, Z.; Zhang, Y. Advanced carbon for flexible and wearable electronics. *Adv. Mater.* **2019**, *31*, No. e1801072.

(7) Guan, H.; Meng, J.; Cheng, Z.; Wang, X. Processing natural wood into a high-performance flexible pressure sensor. *ACS Appl. Mater. Interfaces* **2020**, *12*, 46357−46365.

(8) He, K.; Hou, Y.; Yi, C.; Li, N.; Sui, F.; Yang, B.; Gu, G.; Li, W.; Wang, Z.; Li, Y.; Tao, G.; Wei, L.; Yang, C.; Chen, M. High-performance zero-standby-power-consumption-under-bending pressure sensors for artificial reflex arc. *Nano Energy* **2020**, *73*, No. 104743.

(9) Yi, C.; Hou, Y.; He, K.; Li, W.; Li, N.; Wang, Z.; Yang, B.; Xu, S.; Wang, H.; Gao, C.; Wang, Z.; Gu, G.; Wang, Z.; Wei, L.; Yang, C.; Chen, M. Highly sensitive and wide linear-response pressure sensors featuring zero standby power consumption under bending conditions. *ACS Appl. Mater. Interfaces* **2020**, *12*, 19563−19571.

(10) Gao, L.; Zhu, C.; Li, L.; Zhang, C.; Liu, J.; Yu, H. D.; Huang, W. All paper-based flexible and wearable piezoresistive pressure sensor. *ACS Appl. Mater. Interfaces* **2019**, *11*, 25034−25042.

(11) Yan, J.; Ma, Y.; Li, X.; Zhang, C.; Cao, M.; Chen, W.; Luo, S.; Zhu, M.; Gao, Y. Flexible and high-sensitivity piezoresistive sensor based on MXene composite with wrinkle structure. *Ceram. Int.* **2020**, *46*, 23592−23598.

(12) Chen, S.; Xin, S.; Yang, L.; Guo, Y.; Zhang, W.; Sun, K. Multi-sized planar capacitive pressure sensor with ultra-high sensitivity. *Nano Energy* **2021**, *87*, No. 106178.

(13) Xiong, Y.; Shen, Y.; Tian, L.; Hu, Y.; Zhu, P.; Sun, R.; Wong, C.-P. A flexible, ultra-highly sensitive and stable capacitive pressure sensor with convex microarrays for motion and health monitoring. *Nano Energy* **2020**, *70*, No. 104436.

(14) Hosseini, E. S.; Manjakkal, L.; Shakthivel, D.; Dahiya, R. Glycine-Chitosan-Based Flexible Biodegradable Piezoelectric Pressure Sensor. *ACS Appl. Mater. Interfaces* **2020**, *12*, 9008−9016.

(15) Chen, M.; Li, K.; Cheng, G.; He, K.; Li, W.; Zhang, D.; Li, W.; Feng, Y.; Wei, L.; Li, W.; Zhong, G.; Yang, C. Touchpoint-tailored ultrasensitive piezoresistive pressure sensors with a broad dynamic response range and low detection limit. *ACS Appl. Mater. Interfaces* **2019**, *11*, 2551−2558.

(16) Dong, K.; Peng, X.; Wang, Z. L. Fiber/Fabric-Based piezoelectric and triboelectric nanogenerators for flexible/stretchable and wearable electronics and artificial Intelligence. *Adv. Mater.* **2020**, *32*, No. e1902549.

(17) Ke, K.; McMaster, M.; Christopherson, W.; Singer, K. D.; Manas-Zloczower, I. Highly sensitive capacitive pressure sensors based on elastomer composites with carbon filler hybrids. *Composites, Part A* **2019**, *126*, No. 105614.

(18) Pyo, S.; Choi, J.; Kim, J. Flexible, transparent, sensitive, and crosstalk-free capacitive tactile sensor array based on graphene electrodes and air dielectric. *Adv. Electron. Mater.* **2018**, *4*, No. 1700427.

(19) Kamyshny, A.; Magdassi, S. Conductive nanomaterials for 2D and 3D printed flexible electronics. *Chem. Soc. Rev.* **2019**, *48*, 1712−1740.

(20) Liu, W.; Liu, N.; Yue, Y.; Rao, J.; Cheng, F.; Su, J.; Liu, Z.; Gao, Y. Piezoresistive pressure sensor based on synergistical innerconnect polyvinyl alcohol nanowires/wrinkled graphene film. *Small* **2018**, *14*, No. 1704149.

(21) Luo, C.; Liu, N.; Zhang, H.; Liu, W.; Yue, Y.; Wang, S.; Rao, J.; Yang, C.; Su, J.; Jiang, X.; Gao, Y. A new approach for ultrahigh-performance piezoresistive sensor based on wrinkled PPy film with electrospun PVA nanowires as spacer. *Nano Energy* **2017**, *41*, 527−534.

(22) Mu, J.; Hou, C.; Wang, G.; Wang, X.; Zhang, Q.; Li, Y.; Wang, H.; Zhu, M. An Elastic Transparent Conductor Based on Hierarchically Wrinkled Reduced Graphene Oxide for Artificial Muscles and Sensors. *Adv. Mater.* **2016**, *28*, 9491−9497.

(23) Kim, H.; Lee, S. W.; Joh, H.; Seong, M.; Lee, W. S.; Kang, M. S.; Pyo, J. B.; Oh, S. J. Chemically designed metallic/insulating hybrid nanostructures with silver nanocrystals for highly sensitive wearable pressure sensors. *ACS Appl. Mater. Interfaces* **2018**, *10*, 1389−1398.

(24) Liu, M.-Y.; Hang, C.-Z.; Zhao, X.-F.; Zhu, L.-Y.; Ma, R.-G.; Wang, J.-C.; Lu, H.-L.; Zhang, D. W. Advance on flexible pressure sensors based on metal and carbonaceous nanomaterial. *Nano Energy* **2021**, *87*, No. 106181.

(25) Wu, J.; Li, H.; Lai, X.; Chen, Z.; Zeng, X. Conductive and superhydrophobic F-rGO@CNTs/chitosan aerogel for piezoresistive pressure sensor. *Chem. Eng. J.* **2020**, *386*, No. 123998.

(26) Chen, M.; Wang, Z.; Ge, X.; Wang, Z.; Fujisawa, K.; Xia, J.; Zeng, Q.; Li, K.; Zhang, T.; Zhang, Q.; Chen, M.; Zhang, N.; Wu, T.; Ma, S.; Gu, G.; Shen, Z.; Liu, L.; Liu, Z.; Terrones, M.; Wei, L. Controlled fragmentation of single-atom-thick polycrystalline graphene. *Matter* **2020**, *2*, 666−679.

(27) Bi, L.; Yang, Z.; Chen, L.; Wu, Z.; Ye, C. Compressible AgNWs/Ti3C2Tx MXene aerogel-based highly sensitive piezoresistive pressure sensor as versatile electronic skins. *J. Mater. Chem. A* **2020**, *8*, 20030−20036.

(28) Chao, M.; He, L.; Gong, M.; Li, N.; Li, X.; Peng, L.; Shi, F.; Zhang, L.; Wan, P. Breathable Ti3C2Tx MXene/Protein nano-composites for ultrasensitive medical pressure sensor with degradability in solvents. *ACS Nano* **2021**, *15*, 9746−9758.

(29) Li, Q.; Yin, R.; Zhang, D.; Liu, H.; Chen, X.; Zheng, Y.; Guo, Z.; Liu, C.; Shen, C. Flexible conductive MXene/cellulose nanocrystal coated nonwoven fabrics for tunable wearable strain/pressure sensors. *J. Mater. Chem. A* **2020**, *8*, 21131−21141.

(30) Ma, C.; Yuan, Q.; Du, H.; Ma, M. G.; Si, C.; Wan, P. Multiresponsive MXene (Ti3C2Tx)-decorated textiles for wearable thermal management and human motion monitoring. *ACS Appl. Mater. Interfaces* **2020**, *12*, 34226−34234.

(31) Wang, D.; Wang, L.; Lou, Z.; Zheng, Y.; Wang, K.; Zhao, L.; Han, W.; Jiang, K.; Shen, G. Biomimetic, biocompatible and robust silk Fibroin-MXene film with stable 3D cross-link structure for flexible pressure sensors. *Nano Energy* **2020**, *78*, No. 105252.

(32) Shen, X. Q.; Li, M. D.; Ma, J. P.; Shen, Q. D. Skin-inspired pressure sensor with MXene/P(VDF-TrFE-CFE) as active layer for wearable electronics. *Nanomaterials* **2021**, *11*, No. 716.

(33) Lee, T.; Choi, Y. W.; Lee, G.; Pikhitsa, P. V.; Kang, D.; Kim, S. M.; Choi, M. Transparent ITO mechanical crack-based pressure and strain sensor. *J. Mater. Chem. C* **2016**, *4*, 9947−9953.

(34) Yang, X.; Chen, S.; Shi, Y.; Fu, Z.; Zhou, B. A flexible highly sensitive capacitive pressure sensor. *Sens. Actuators, A* **2021**, *324*, No. 112629.

(35) Chen, J.; Yu, Q.; Cui, X.; Dong, M.; Zhang, J.; Wang, C.; Fan, J.; Zhu, Y.; Guo, Z. An Overview of Stretchable Strain Sensors from Conductive Polymer Nanocomposites. *J. Mater. Chem. C* **2019**, *7*, 11710−11730.

(36) Dai, X.; Huang, L.-B.; Du, Y.; Han, J.; Kong, J. Self-healing flexible strain sensors based on dynamically cross-linked conductive nanocomposites. *Compos. Commun.* **2021**, *24*, No. 100654.

(37) Hwang, J.; Kim, Y.; Yang, H.; Oh, J. H. Fabrication of hierarchically porous structured PDMS composites and their application as a flexible capacitive pressure sensor. *Composites, Part B* **2021**, *211*, No. 108607.

(38) Ma, L.; Shuai, X.; Hu, Y.; Liang, X.; Zhu, P.; Sun, R.; Wong, C.-p. A Highly Sensitive and Flexible Capacitive Pressure Sensor Based on A Micro-arrayed Polydimethylsiloxane Dielectric Layer. *J. Mater. Chem. C* **2018**, *6*, 13232−13240.

(39) Zhu, Y.; Wu, Y.; Wang, G.; Wang, Z.; Tan, Q.; Zhao, L.; Wu, D. A flexible capacitive pressure sensor based on an electrospun polyimide nanofiber membrane. *Org. Electron.* **2020**, *84*, No. 105759.

(40) Kim, S. J.; Mondal, S.; Min, B. K.; Choi, C. G. Highly sensitive and flexible strain-pressure sensors with cracked paddy-shaped MoS2/Graphene Foam/Ecoflex hybrid nanostructures. *ACS Appl. Mater. Interfaces* **2018**, *10*, 36377−36384.

(41) Chen, M.; Xia, J.; Zhou, J.; Zeng, Q.; Li, K.; Fujisawa, K.; Fu, W.; Zhang, T.; Zhang, J.; Wang, Z.; Wang, Z.; Jia, X.; Terrones, M.;

Shen, Z. X.; Liu, Z.; Wei, L. Ordered and atomically perfect fragmentation of layered transition metal dichalcogenides via mechanical instabilities. *ACS Nano* **2017**, *11*, 9191−9199.

(42) Yu, P.; Li, X.; Li, H.; Fan, Y.; Cao, J.; Wang, H.; Guo, Z.; Zhao, X.; Wang, Z.; Zhu, G. All-fabric ultrathin capacitive sensor with high pressure sensitivity and broad detection range for electronic skin. *ACS Appl. Mater. Interfaces* **2021**, *13*, 24062−24069.

(43) Zhang, Q.; Wang, Y. L.; Xia, Y.; Kirk, T. V.; Chen, X. D. Textile-Only capacitive sensors with a lockstitch structure for facile integration in any areas of a fabric. *ACS Sens.* **2020**, *5*, 1535−1540.

(44) Huang, Y.; Wang, Z.; Zhou, H.; Guo, X.; Zhang, Y.; Wang, Y.; Liu, P.; Liu, C.; Ma, Y.; Zhang, Y. Highly sensitive pressure sensor based on structurally modified tissue paper for human physiological activity monitoring. *J. Appl. Polym. Sci.* **2020**, *137*, No. 48973.

(45) Li, F.; Liu, Y.; Shi, X.; Li, H.; Wang, C.; Zhang, Q.; Ma, R.; Liang, J. Printable and stretchable temperature-strain dual-sensing nanocomposite with high sensitivity and perfect stimulus discrim-inability. *Nano Lett.* **2020**, *20*, 6176−6184.

(46) Li, T.; Chen, L.; Yang, X.; Chen, X.; Zhang, Z.; Zhao, T.; Li, X.; Zhang, J. A Flexible Pressure Sensor Based on An MXene−Textile Network Structure. *J. Mater. Chem. C* **2019**, *7*, 1022−1027.

(47) Kannichankandy, D.; Pataniya, P. M.; Narayan, S.; Patel, V.; Sumesh, C. K.; Patel, K. D.; Solanki, G. K.; Pathak, V. M. Flexible piezo-resistive pressure sensor based on conducting PANI on paper substrate. *Synth. Met.* **2021**, *273*, No. 116697.

(48) Li, T.; Luo, H.; Qin, L.; Wang, X.; Xiong, Z.; Ding, H.; Gu, Y.; Liu, Z.; Zhang, T. Flexible capacitive tactile sensor based on micropatterned dielectric layer. *Small* **2016**, *12*, 5042−5048.

(49) Zhou, Q.; Ji, B.; Wei, Y.; Hu, B.; Gao, Y.; Xu, Q.; Zhou, J.; Zhou, B. A bio-inspired cilia array as the dielectric layer for flexible capacitive pressure sensors with high sensitivity and a broad detection range. *J. Mater. Chem. A* **2019**, *7*, 27334−27346.

(50) Zhang, Y.; Liu, S.; Miao, Y.; Yang, H.; Chen, X.; Xiao, X.; Jiang, Z.; Chen, X.; Nie, B.; Liu, J. Highly stretchable and sensitive pressure sensor array based on icicle-shaped liquid metal film electrodes. *ACS Appl. Mater. Interfaces* **2020**, *12*, 27961−27970.

(51) Li, W.; Jin, X.; Zheng, Y.; Chang, X.; Wang, W.; Lin, T.; Zheng, F.; Onyilagha, O.; Zhu, Z. A porous and air gap elastomeric dielectric layer for wearable capacitive pressure sensor with high sensitivity and a wide detection range. *J. Mater. Chem. C* **2020**, *8*, 11468−11476.

(52) Sharma, S.; Chhetry, A.; Sharifuzzaman, M.; Yoon, H.; Park, J. Y. Wearable Capacitive Pressure Sensor Based on MXene Composite Nanofibrous Scaffolds for Reliable Human Physiological Signal Acquisition. *ACS Appl. Mater. Interfaces* **2020**, *12*, 22212−22224.